1   **Cesium Adsorption Isotherm on Swelling High-charged Micas**

2   **from Aqueous Solutions: Effect of Temperature**

3   Francisco J. Osuna,[a] Agustín Cota,[b] Esperanza Pavón,[c] M. Carolina Pazos[d] and María D.

4   Alba.[a,1]

5   [a]Instituto Ciencia de Materiales de Sevilla (CSIC-Universidad de Sevilla). Avda.

6   Américo Vespucio, 49.41092 Sevilla, Spain

7   [b]Laboratorio de Rayos-X. CITIUS. Avda. Reina Mercedes, 4. 41012 Sevilla, Spain

8   [c]Center for the Development of Nanoscience and Nanotechnology, CEDENNA,

9   9170124 Santiago, Chile

10 [d]Escuela de Ciencias Químicas, Universidad Pedagógica y Tecnológica de Colombia

11 UPTC. Avda. Central del Norte, Vía Paipa, Tunja, 39-115 Boyacá, Colombia.

12

13   **ABSTRACT**

14   The potential use of a new family of synthetic swelling micas for cesium

15 immobilization from aqueous solution was evaluate and the structural modifications

16 after adsorption were analyzed. The results have revealed that they are good cesium

17 adsorbents compared to natural clays and as the layer charge increases, the adsorption

18 capacity and affinity increase. The cesium ions are adsorbed through a cation exchange

19 mechanism but an inner sphere complex with the basal oxygens of the tetrahedral sheet

20 is favored. These findings imply that is possible to design minerals with improved

21 environmental applications.

22

23

[1] Corresponding author: *e-mail address:* alba@icmse.csic.es

24   **Keywords:** Cesium aqueous solution; synthetic mica; sorption isotherm; clay barrier;

25   waste management

26

27   **INTRODUCTION**

28   Along with the rapid development of nuclear industries, the contamination of

29   radionuclides in the environment is a point of attention worldwide (Steinhauser 2014).

30   Cesium isotopes (^{137}Cs, $t_{1/2}$= 30 yr, and ^{135}Cs, $t_{1/2}$= $2 \cdot 10^6$ yr) are one of the major

31   constituents of the wastewater effluents from nuclear reprocessing units (Castrillejo et

32   al. 2016) and due to their long half-lives and high solubility, they are the most

33   hazardous nuclides in radioactive wastes. Given its chemical similarity to alkalis, Cs^+ is

34   readily assimilated by terrestrial and aquatic organisms and can gradually accumulate in

35   the biological food chain (Nakao et al. 2008; Poinssot et al. 1999). Cesium strongly and

36   selectively interacts with the phyllosilicate fraction of soil, sediment, and suspended

37   particles (Zachara et al. 2002) but the interaction of Cs^+ in a geological material is

38   expected to be highly sensitive to the relative compositions of smectite/vermiculite and

39   mica/illite (Fan et al. 2014).

40   The objective of any waste management is immobilization and isolation for the time

41   necessary to lower its environmental activity and for this, a number of natural and

42   artificial barriers are used. Numerous studies focused on using clays as a chemical

43   barrier for retention and storage of radioactive materials have been reported, since they

44   have a great capacity to adsorb and immobilize cations (Alba et al. 2001; Chorover et al.

45   2003; Rani and Sasidhar 2012; Takahashi et al. 1987; Villa-Alfageme et al. 2015).

46   Clayey waste materials can retain radionuclides by sorption but also, under certain

47   conditions, can produce a chemical reaction that generates new phases immobilizing the

48   radioactive elements (Villa-Alfageme et al. 2015). Other features that make clays useful

49   for retention of radioactive waste are their low permeability and high swelling capacity

50   for absorption of ions, which predetermine their use as sealing barriers in multi-barrier

51   systems when an underground geological repository for spent nuclear fuel and high-

52   level radioactive wastes is constructed (Linares 1993).

53   Up to now, bentonites (smectites ca. 90%) have been proposed as the best candidate

54   for the barriers (Gregor 1969). The principal component of bentonites is a 2:1 layer

55   phyllosilicate with lamellar charge between 0.2 and 0.8. It is well known that as the

56   total charge increases the immobilization capacity of the clay increases (Weir 1965).

57   Structural features that increase the reactivity of these 2:1 phyllosilicates are the

58   presence of aluminum in the tetrahedral sheet and the total occupation of the octahedral

59   sheet (Alba et al. 2001). In this sense, Alba et al. (Alba et al. 2006) have synthesized a

60   swelling high-charged (4 eq/unit cell) mica, Na-Mica-4, which is able to rehydrate and

61   swell and has a high cation exchange capacity, comparable to aluminum-rich zeolites.

62   These micas have attracted considerable interest because of their exceptional adsorption

63   capacity and selectivity of harmful cations (Alba et al. 2006; Franklin and Lee 1996;

64   Garcia-Jimenez et al. 2016; Kodama et al. 2001; Paulus et al. 1992) and they constitute

65   a promising material for Cs adsorption.

66   Hence, the aim of this study was: (i) to evaluate the potential use of synthetic

67   swelling high-charged micas, Na-Mica-n (n=2 and 4, layer charge) for cesium

68   immobilization at standard temperature and pressure conditions; (ii) to evaluate the

69   effect of temperature on its adsorption capacity; and; (iii) to determine the adsorption

70   mechanism (unspecific adsorption or specific adsorption) that occurs at different

71   temperatures.

72

73

74   **EXPERIMENTAL AND ANALYTICAL PROCEDURES**

75 **Chemicals and materials**

76   Na-Mica-n (n = 2 and 4) was synthesized using the NaCl-melt method following a

77 similar procedure to that described by Alba et al. (Alba et al. 2006). Their structural

78 formulae are $Na_n[Si_{8-n}Al_n]Mg_6O_{20}F_4$, where *n* represents the charge per unit cell (n = 2

79 and 4). The starting materials employed were SiO_2, $Al(OH)_3$, MgF_2 and NaCl.

80 Stoichiometric proportions of reactants were weighed and mixed in an agate mortar.

81 The molar ratio between the reactants were $(8-n)SiO_2:(n/2)Al_2O_3:6MgF_2:(2n)NaCl$

82 (Alba et al. 2006). The heat treatments were carried out in closed Pt crucibles at 900 ºC

83 over 15 h using a heating rate of 10 $ºC·min^{-1}$. The product was washed with distilled

84 water and the solid was separated by filtration, dried at room temperature and then

85 ground in an agate mortar.

86

87 **Sorption equilibrium isotherm**

88   Each batch test sample in the sorption experiments at room temperature (RT) was

89 prepared in a 50 ml centrifuge tube, where 0.2 g of Na-Mica-4 was dispersed with 30 ml

90 of a CsCl solution at different concentrations ranging between 0.01-25 meq/L, the

91 maximum concentration allows for satisfying the theoretical cation exchange capacity

92 of the Na-Mica-4. For comparison, an adsorption at an initial concentration of 1 meq/L

93 was carried out in Na-Mica-2. The samples were equilibrated for 24 h in an end-over-

94 end shaker at 50 r.p.m. The phases were separated by centrifugation at 10,000 rpm at 8

95 ºC for 25 min.

96   The sorption isotherm at 80 ºC was carried out in a hydrothermal bomb (Alba et al.

97 2006) where 0.2 g of Na-Mica-4 was mixed with 30 ml of a CsCl solution at different

98 concentrations ranging between 1.5-25 meq/L and heated at 80 ºC for 24 h.

99   The supernatants were preserved by adding HNO_3 and cool stored for subsequent Cs^+

100   analysis by inductively coupled plasma-mass spectrometry (ICP-MS). The difference

101   between Cs^+ concentrations measured before and after sorption reveals the amount of

102   adsorbed Cs^+ (C_s, meq/kg)

103
$$C_s = \left(C_i - C_{eq} \right) \cdot \frac{V}{m}$$

104   where the V (L) is the volume of the solution, m is the weight of the mica (kg), C_i

105   (meq/L) and C_{eq} (meq/L) are the concentration of the Cs^+ in initial and final solutions,

106   respectively.

107   The solids were dried at room temperature and characterized by X-ray diffraction

108   (XRD), SEM/EDX microscopy and MAS NMR spectroscopy.

109   The adsorption percentage and the distribution ratio (K_d, L/kg), were calculated as

110   follows:

111
$$\% \, Adsorption = \frac{C_i - C_{eq}}{C_i} \cdot 100$$

112
$$K_d = \frac{C_s}{C_{eq}}$$

113   The Freundlich adsorption isotherm is widely used for mathematical descriptions of

114   adsorption on a heterogeneous adsorbent surface (Veli and Alyuz 2007). This isotherm

115   gives an expression encompassing the surface heterogeneity and the exponential

116   distribution of active sites and their energy. It can be written as follows (Bhattacharyya

117   and Sen Gupta 2007):

118
$$C_s = K_F \cdot C_{eq}{}^{n_F}$$

119   K_F (L/kg) is the Freundlich constant, which is related to adsorption capacity, and n_F

120   (dimensionless) is the adsorption intensity. The Freundlich constant n_F is a measure of

121   the deviation from linearity adsorption ($n_F=1$). If n_F value is above 1, this implies that

122   the sorption process is chemical, but if n_F value is below 1, sorption is more likely a

123   physical process (Xi et al. 2014). The physical adsorption is that where the interaction

124   between cesium and the mica surface is through weak Van der Waals forces (i.e. cation-

125   exchanged reaction). However, if the cesium reacts with the mica, the adsorption

126   mechanism is through ionic bonding. In general, the chemical adsorption requires

127   higher temperatures than the physical one.

128

129   **Characterization Techniques**

130   The Cs^+ concentrations in the initial and final solutions were measured by ICP-

131   MS with an atomic emission spectrometer with inductively coupled source, Perkin

132   Elmer, Model DRC-e. Such equipment is settled in the Mass Spectrometry and

133   Chromatography Unit at the University of Cordoba, Spain.

134   X-ray diffraction (XRD) patterns were obtained at the CITIUS X-ray laboratory

135   (University of Seville, Spain) on a Bruker D8 Advance instrument equipped with a Cu

136   Kα radiation source operating at 40 kV and 40 mA. Diffractograms were obtained in the

137   2θ range of 3–70° with a step size of 0.015° and a step time of 0.1 s.

138   The morphology and elemental composition of the crystalline phases after the Cs

139   treatments were analyzed by scanning electron microscopy (SEM/EDX), using a JEOL

140   microscope (JSM 5400 Model) and working at 20 kV, which is installed in the

141   Microscopy Service of ICMS (CSIC-US). This equipment is connected to an energy

142   dispersive system X-ray (EDX) (Oxford Link ISIS) which allows chemical analysis of

143   samples using a detector of Si/Li with a Be window.

144   The analysis of short-range structural order was carried out by Solid State Magic

145   Angle Spinning-Nuclear Magnetic Resonance (MAS-NMR). Spectra were acquired

146   using single pulse programs on a Bruker DRX 400, equipped with a multinuclear probe.

147   Solid samples were packed in cylindrical zirconia rotors of 4 mm diameter and turned

148   under the magic angle at a frequency of 10 kHz. ^{29}Si spectra were acquired at a

149   frequency of 79.49 MHz, using pulse width values of 2.66 µs ($\pi/2$ = 7.98 µs), and a

150   delay time of 3 s. The chemical shift values were expressed in ppm, using

151   tetramethylsilane as an external reference.

152

153   **RESULTS**

154

155   The adsorbed amounts of Cs^+ and K_d values of the different scenarios have been

156   obtained from the ICP-MS analysis. Figure 1 shows a comparison of the adsorption

157   percentage and K_d values with temperature. The variation of adsorption percentage on

158   Na-Mica-4 versus the initial concentration (Fig 1a) shows a maximum adsorption of

159   80% at low concentrations that decreased with an increase of the initial concentration,

160   whereas the K_d values (Fig. 1b) decreased exponentially with increasing adsorbed

161   cesium.

162   At 80 °C, as at RT, the adsorption percentage and the K_d values decreased when

163   the initial solution concentration and adsorbed cesium increased. However, at 80 °C a

164   higher adsorption was observed at nonspecific sites but with higher affinity (low K_d

165   values, but higher than at RT) was observed (Galunin et al. 2010). This difference was

166   greater at low initial concentrations, at C_i=1.5 meq/L: K_d (L/kg)=311.1±13.60 (RT) vs

167   548.1± 4.66 (80 ºC) and % ads= 67.5±4.03 (RT) vs 78.5±0.14 (80 ºC). At the higher

168   initial concentration, the opposite occurred, at C_i=25.0 meq/L: K_d (L/kg)=91.4±3.95

169   (RT) vs 78.8±4.58 (80 ºC) and % ads= 37.9±1.83 (RT) vs 34.5± 1.31 (80 ºC).

170   The adsorption isotherm at both temperatures for Na-Mica-4 (Fig. 2) fitted to an

171   L-Type isotherm without a plateau being formed and, thus, the adsorption limits were

172   not reached (Limousin et al. 2007). In fact, the maximum value of adsorption was ca.

173   1587.7 meq/kg at RT and ca. 2307.6 meq/kg at 80 ºC, which is below the cation

174   exchange capacity of 4694.8 meq/kg.

175   The SEM micro-scale images (Fig. 3) show that mica retained its laminar

176   structure and, therefore, the adsorption did not cause delamination of the clay, a

177   postulated mechanism by some authors (Vejsada et al. 2005), when Na^+ was exchanged

178   by other alkaline cations of higher radius such as K^+. The swelling state of the layers

179   was analyzed by XRD, and the XRD patterns of the samples after the adsorption (Fig.

180   4) showed *00l* reflections compatible with a basal spacing of 1.20-1.22 nm, which

181   indicated that Cs^+ formed a hydration complex in the interlayer space (Alba et al. 2006).

182   At both temperatures, a decrease of the basal space was observed with respect to Na-

183   Mica-4 when the initial Cs^+ concentration increased. Even at 80 ºC, no XRD reflections

184   due to formation of new crystalline phases were observed (Fig. 5).

185   In the case of samples after adsorption of cesium at 80 ºC, a study by ^{29}Si MAS

186   NMR (Fig. 6) was carried out in order to detect if the temperature could favor the

187   nucleation of new phases that could not be observed by XRD. The initial Na-Mica-4

188   spectrum showed a set of signals between -75 and -100 ppm due to $Q^3(nAl)$ with n=0, 1,

189   2 and 3 environments typical of micas (Sanz and Serratosa 1984). After adsorption at 80

190   ºC, the same set of signals with a gradual shift towards lower frequencies was observed.

191

192   **DISCUSSION**

193

194   The moderate K_d values indicated adsorption predominantly in nonspecific sites

195   (Galunin et al., 2010) but the observation that it exponentially decreases with increasing

196   adsorbed cesium (Fig. 1b) could indicate that there are interlayer adsorption sites of

197   different specificity (Sposito et al., 1999):

198   - Site I: High affinity sites: the interlayer cation could form inner-sphere

199   complexes by partial incorporation into the pseudo-hexagonal holes of the

200   tetrahedral sheet..

201   - Site II: Low-affinity sites: the interlayer cation could form outer-sphere

202   complexes as a hydrated interlayer cation.

203   Figure 1b shows that at low concentrations of adsorbed cesium the adsorption in

204 the high-affinity site is higher at 80 ºC than at RT (higher K_d values) because the

205 temperature favors the interaction with basal oxygens and an inner-sphere complex

206 being favored. However, the observed convergence of K_d values where high adsorbed

207 cesium is indicated, inferred that the adsorption on site II occurred after all of site I was

208 occupied.

209   In order to evaluate the adsorption capacity of the synthetic high-charged micas

210 (Na-Mica-n) with conventional adsorbents and to analyze the effect of the layer charge,

211 Table 1 summarizes the adsorption values obtained from the Na-Mica-n and from the

212 natural clays (Galambos et al. 2009; García-Gutiérrez 2010; Oztop and Shahwan 2006;

213 Saxena et al. 2003). First, it was noted that synthetic micas, Na-Mica-n, adsorbed more

214 Cs^+ than some of the natural clays. This result is remarkable considering that the

215 experimental conditions in the case of micas are unfavorable since the ratio

216 adsorbent:solution (S/L, g/L) is much higher in the case of natural clay assays (Wu et al.

217 2009). When comparing the percentage of adsorption between both synthetic micas

218 studied here, a major adsorption capacity was observed as the lamellar charge increased

219 (Na-Mica-4 > Na-Mica-2). In all cases, the main adsorption mechanism was in

220 nonspecific sites and, thus, the adsorption capacity was governed by the mineral cation

221 exchange capacity (CEC).

9

222   Comparing the K_d values of Na-Mica-n and those from the literature (Table 1)

223   shows that the specificity of the adsorption sites on the Na-Mica-4 are higher than those

224   of Na-Mica-2, which can be justified because the cation amount necessary to satisfy the

225   charge is half of that required in Na-Mica-2. Thus, the cations in Na-Mica-2 has less

226   interaction with basal oxygens, as demonstrated by the analysis of the *b*-parameter

227   values of the unit cell (Pavon et al. 2014). In general, the K_d values of Na-Mica-4 were

228   higher than natural clays and fluoro-phlogopite gel, even when the ratio of

229   adsorbent:solution (g/l) was much lower. In some cases, the initial concentration was

230   much higher in the case of Na-Mica-n, both being unfavorable conditions for the

231   adsorption parameters (Wu et al. 2009).

232   The maximum value of adsorption at both temperatures (RT and 80˚C; Fig. 2)

233   was below the cation exchange capacity of Na-Mica-4. This fact has been previously

234   observed with alkali cations, specifically, Park et al. (Park et al., 2012a) observed that

235   when Na-Mica-4 was subjected to a process of cation exchange with K^+ or Rb^+ only

236   half of the Na^+ was replaced, hydronium ions were generated and they only partially

237   balanced the layer charge. In fact, the EDX composition map (Fig; 3) showed that the

238   distribution of cesium was similar to that of sodium indicating that the cesium replaced

239   the sodium in the interlayer space, although not completely. This reinforces that the

240   adsorption of cesium is by a cation exchange mechanism as previously reported, and in

241   accordance with the low K_d values.

242   An in depth analysis of the isotherm data was performed using the Freundlich

243   model (Table 2) and the experimental data fit to two lines with different slopes

244   supporting the two aforementioned interpretation of adsorption sites (Vejsada et al.,

245   2005):

246   -Site I: The K_F values were high at both temperatures; at 80 ºC being higher,

247   which indicates that the site I was a site of high adsorption affinity. The n_F value at RT

248   was close to one which denotes a uniformity of the surface, which drastically

249   diminishes at 80 ºC. The diminishing of n_F with temperature indicates that the

250   adsorption bonds become weak at high temperature, and thus the cesium adsorption on

251   site I is exothermic (Xi et al., 2014).

252   - Site II: The K_F values are lower than those in site I at both temperatures; at 80

253   ºC being even lower, which indicates that the site II was a site of lower adsorption

254   affinity and corresponds to adsorption in the outer sphere as an interlayer hydrated

255   cation. The n_F value at both temperatures was ca. 0.65 which shows that the clay surface

256   charge is heterogeneous.

257   In both sites, the n_F values were lower than the unit, which indicates that the

258   adsorption is by a physical process, through a cation exchange mechanism in sites with

259   variable cation affinity (Harter and Baker 1977). Freundlich type sorption implies that

260   there are at least two distinct sorption sites for Cs^+ as on illite (Poinssot et al. 1999). The

261   "frayed edge" site, site I, dominates Cs^+ uptake at low concentration and the Na^+ ions

262   compete but only at concentrations of orders of magnitude higher than Cs^+. Such sites

263   are common in illite but are not generally associated with other clay minerals (Bradbury

264   and Baeyens 2000). The second class of site (Site II) is the "planar site" (basal siloxane

265   surface) and it is associated with the fixed negative charge on the tetrahedral sheet.

266   If we compare these data with those of natural clays, (Table 3) the Na-Mica-4

267   exhibited higher values of the K_F constant. Therefore, the Na-Mica-4 have greater

268   affinity for cesium adsorption (Turiel et al., 2003). Moreover, the adsorption surface of

269   Na-Mica-4 is more homogeneous than that of natural clays.

270   After adsorption at high concentration, the basal spacing of the layered structure

271   diminishes due to the lower hydration energy of cesium (264 kJ/mol) versus sodium

272   (519 kJ/mol), which favors the formation of inner complexes with the basal oxygen for

273   Cs^+ (Anderson and Sposito 1991, 1992). The absence of new phases containing cesium

274   documented by XRD (Fig. 5) and ^{29}Si MAS NMR (Fig. 6) agrees with the n_F values that

275   indicate Cs^+ was bonded by weak electrostatic (Van der Waals) interactions.

276   However, the gradual shift of the set of ^{29}Si MAS NMR signals towards lower

277   frequencies indicates a participation of the inner-sphere complex. Those complexes

278   imply that cesium is partially located in the pseudo-hexagonal holes of the tetrahedral

279   sheet, interacting with the basal oxygens, and, thus, modifying the angle of rotation of

280   the tetrahedra (Limousin et al. 2007).

281

282   **IMPLICATIONS**

283

284   We have demonstrated that synthetic micas, Na-Mica-n, are better adsorbents of

285   cesium from aqueous solution than natural clays. The adsorption capacity and affinity

286   increases as the layer charge of micas increase. The cesium isotherm followed the

287   Freundlich model and the fit parameters pointed to a physical adsorption by a cation

288   exchange mechanism at both temperatures. At higher temperature (80°C) an increase of

289   the Cs-adsorption was observed in higher affinity sites without actually modifying the

290   mica structure, because the adsorption is thorough cation exchange but with higher

291   participation of the inner-sphere complex. These results show that minerals can be

292   designed with improved environmental applications.

293

294

295

ACKNOWLEDGEMENTS

297

306

307

308

TABLE 1. Adsorption parameters for Cs^+ sorption on Na-Mica-n (n=2 and 4) and natural clays at RT.

	C_i meq/L	S/L[a] g/ml	K_d L/kg	% Ads.	Ref.
Na-Mica-4	10^{-2}	$7 \cdot 10^{-3}$	549.2	78.5	b
	1	$7 \cdot 10^{-3}$	367.5	71.0	b
Na-Mica-2	10^{-2}	$7 \cdot 10^{-3}$	396.5	68.1	b
Bentonite Rojo carbonero	$3 \cdot 10^{-6}$	$1 \cdot 10^{-1}$	497.0	--	c
Sediment St. Juan (Huelva)	$3 \cdot 10^{-6}$	$1 \cdot 10^{-1}$	664.0	--	c
Sepiolite	$3 \cdot 10^{-6}$	$1 \cdot 10^{-1}$	381.7	--	c
Fluorphlogopite	10^{-2}	$2 \cdot 10^{-2}$	80	--	d
gel	1	$2 \cdot 10^{-2}$	63	--	d
Clay MI	1	$1 \cdot 10^{-2}$	--	44.0	e
Clay MIS	1	$1 \cdot 10^{-2}$	--	65.0	e
Clay MID	1	$1 \cdot 10^{-2}$	--	89.0	e
Bentonite J45	1	$1 \cdot 10^{-2}$	785	72	f
Bentonite K45	1	$1 \cdot 10^{-2}$	478	72	f
Bentonite L45	1	$1 \cdot 10^{-2}$	296	36	f
Bentonite LA45	1	$1 \cdot 10^{-2}$	214	32	f

[a] the ratio adsorbent:solution
[b] this work; [c] (García-Gutiérrez 2010); [d] (Saxena et al. 2003);
[e] (Oztop and Shahwan 2006); [f] (Galambos et al. 2009)

309

310

TABLE 2. Parameters from Freundlich isotherm equation for the adsorption of Cs^+ on Na-Mica-4, at RT and 80 ºC.

T (ºC)	Site I			Site II		
	K_F L/kg	n_F	R^2	K_F L/kg	n_F	R^2
RT	288.14±1.09	0.90±0.02	0.996	235.70±1.04	0.63±0.03	0.992
80	336.59±1.02	0.57±0.03	0.995	219.72±1.15	0.65±0.05	0.989

311

312

313

TABLE 3. Parameters from Freundlich isotherm equations for the adsorption of Cs^+ on natural clays.

	K_F L/kg	n_F	Ref.
SAMMS	$2.18 \cdot 10^{-4}$	0.45	[a]
SAz-1	176.00	0.91	[b]
S-Tx-1	60.68	0.84	[b]
IMt-1	1.63	0.61	[b]
KGa-2	0.70	0.67	[b]
Mont-Ill-MI	2.95	0.52	[c]
Mont-Ill-MIS	12.00	0.62	[c]
Mont-Ill-MID	63.10	0.69	[c]

[a] (Park et al. 2012); [b] (Vejsada et al. 2005); [c] (Nakao et al. 2008; Oztop and Shahwan 2006)

314

315

316

FIGURE CAPTIONS

FIGURE 1. Cs^+ adsorption on Na-Mica-4, at RT (white circle) and 80º C (black star):

a) Adsorption percentage, and, b) K_d.

FIGURE 2. Adsorption isotherm of Cs^+ on Na-Mica-4 at RT (white circle) and 80 ºC

(black star).

FIGURE 3. SEM microimage and compositional maps of Na-Mica-4 after Cs^+ sorption

at a) RT, and, b) 80 ºC.

FIGURE 4. *001* reflection of Na-Mica-4 before and after Cs^+ adsorption at a) RT, and,

b) 80 ºC.

FIGURE 5. Full XRD patterns of Na-Mica-4 before (marked as M4) and after Cs^+

adsorption at 80º C at the indicated initial concentration. Oriented clay mounts in air-

dried form (Cu kα radiation).

FIGURE 6. ^{29}Si MAS NMR spectra of Na-Mica-4 before and after Cs^+ sorption at 80

ºC.

336

Figure 1

337
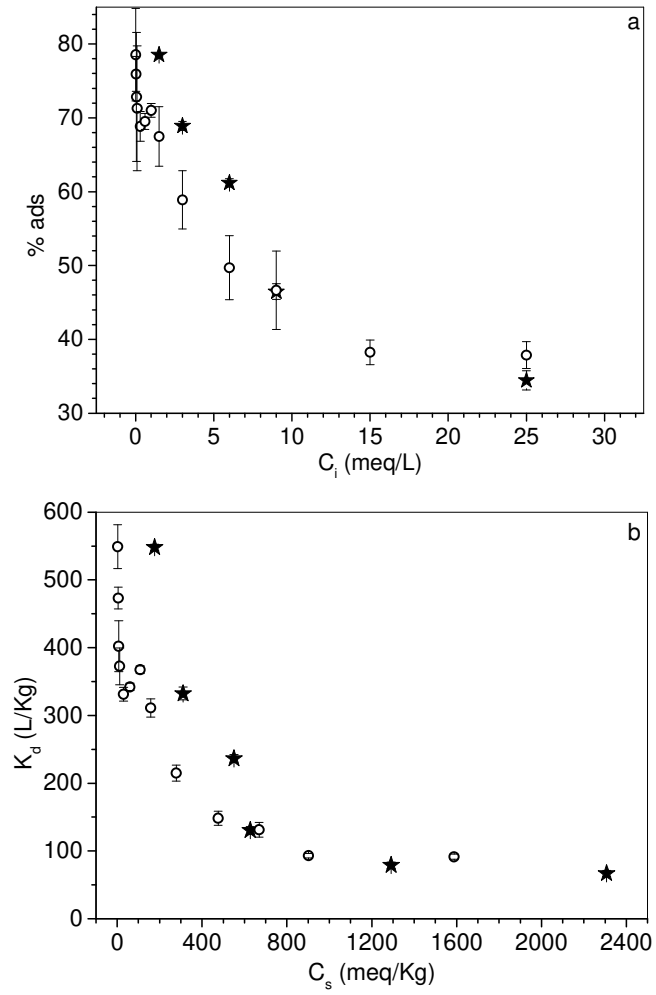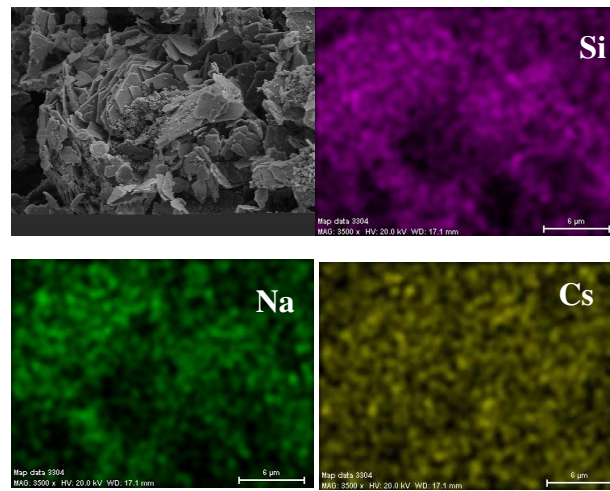
338

Figure 2

339

340

Figure 3

341

a

b

342

Figure 4

343

344

345 *Figure 5*

346

347

348 *Figure 6*

349

[Cs⁺]ᵢ meq/L

50

25

9.0

6.0

3.0

1.5

0

^{29}Si (ppm)

-70 -75 -80 -85 -90 -95 -100
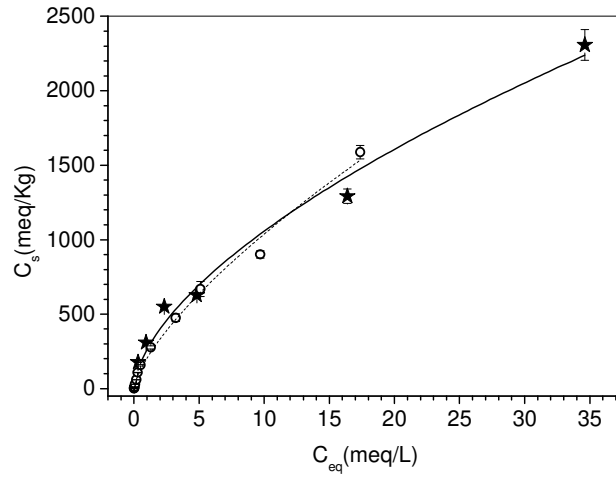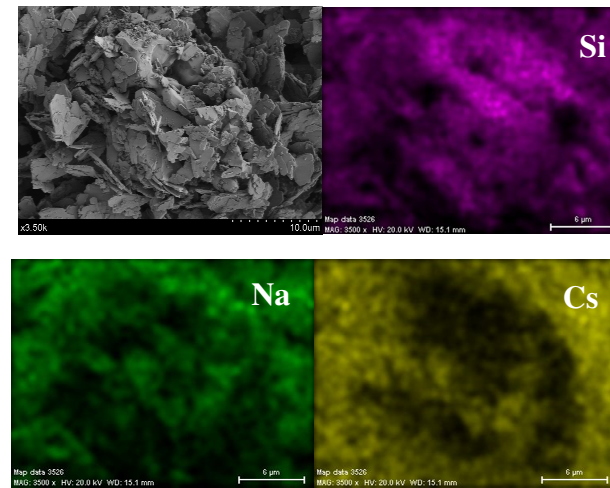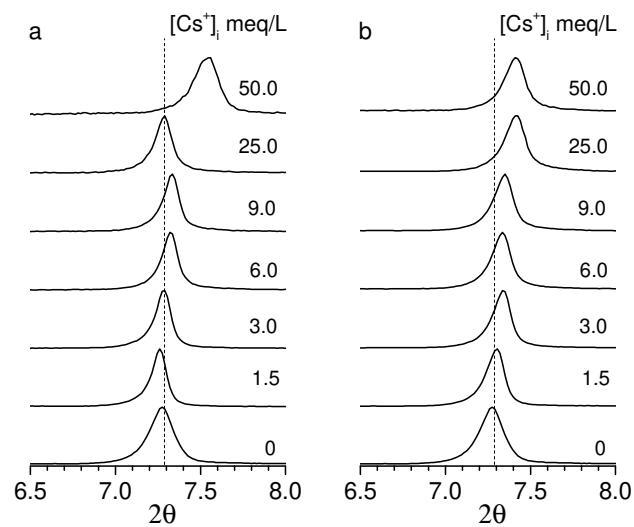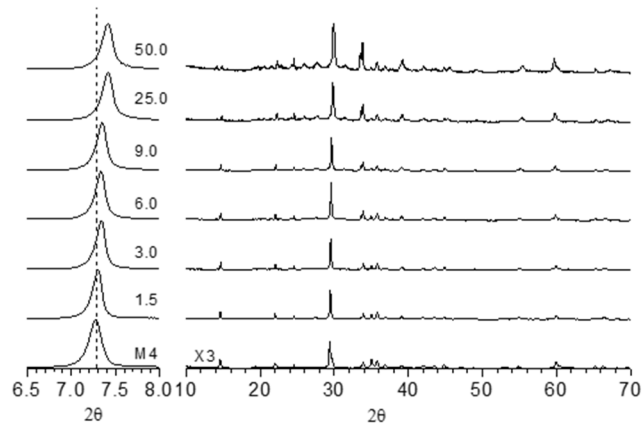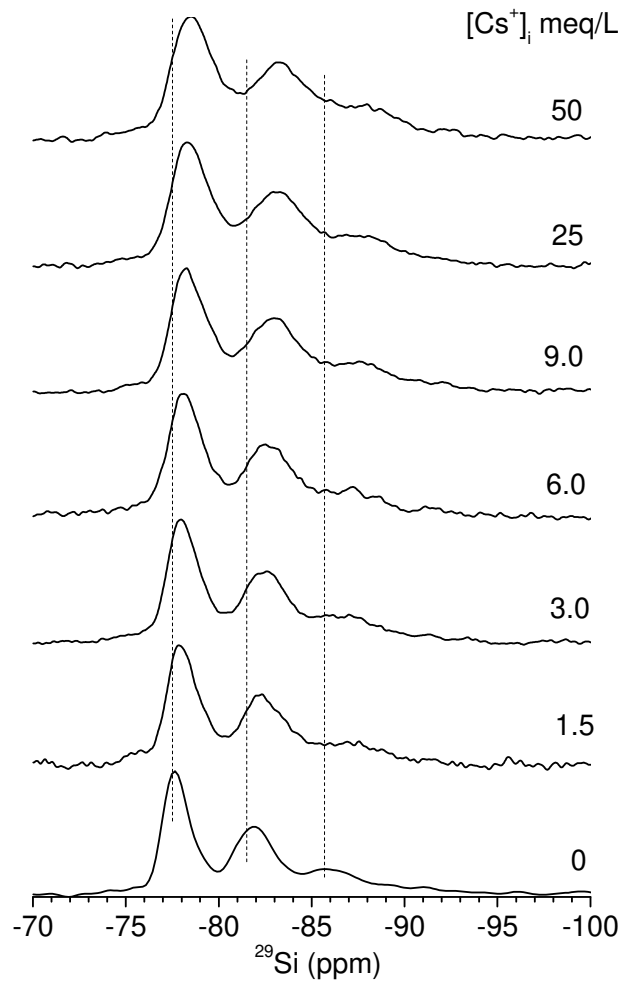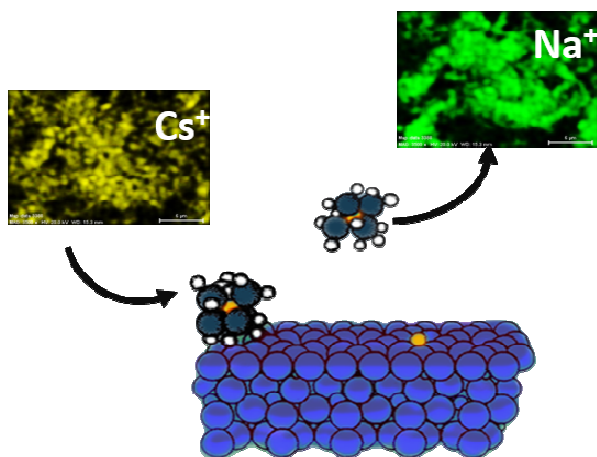
350 **GRAPHICAL ABSTRACT**

351

352

353

REFERENCES CITED

354

355

356 Alba M.D., Becerro A.I., Castro M.A. and Perdigon A.C. (2001) Hydrothermal

357   reactivity of Lu-saturated smectites: Part II. A short-range order study. Am.

358   Miner. 86, 124-131.

359 Alba M.D., Castro M.A., Naranjo M. and Pavon E. (2006) Hydrothermal reactivity of

360   Na-n-micas (n=2, 3, 4). Chem. Mat. 18, 2867-2872.

361 Anderson S.J. and Sposito G. (1991) Cesium-adsorption method for measuring

362   accessible structural surface-charge. Soil Sci. Soc. Am. J. 55, 1569-1576.

363 Anderson S.J. and Sposito G. (1992) Proton surface-charge density in soils with

364   structural and ph-dependent charge. Soil Sci. Soc. Am. J. 56, 1437-1443.

365 Bhattacharyya K.G. and Sen Gupta S. (2007) Adsorptive accumulation of Cd(II),

366   Co(II), Cu(II), Pb(II), and Ni(II) from water on montmorillonite: Influence of

367   acid activation. J. Colloid Interface Sci. 310, 411-424.

368 Bradbury M.H. and Baeyens B. (2000) A generalised sorption model for the

369   concentration dependent uptake of caesium by argillaceous rocks. J. Contam.

370   Hydrol. 42, 141-163.

371 Castrillejo M., Casacuberta N., Breier C.F., Pike S.M., Masque P. and Buesseler K.O.

372   (2016) Reassessment of Sr-90, Cs-137, and Cs-134 in the Coast off Japan

373   Derived from the Fukushima Dai-ichi Nuclear Accident. Environ. Sci. Technol.

374   50, 173-180.

375 Chorover J., Choi S.K., Amistadi M.K., Karthikeyan K.G., Crosson G. and Mueller

376   K.T. (2003) Linking cesium and strontium uptake to kaolinite weathering in

377   simulated tank waste leachate. Environ. Sci. Technol. 37, 2200-2208.

378 Fan Q.H., Tanaka M., Tanaka K., Sakaguchi A. and Takahashi Y. (2014) An EXAFS
379   study on the effects of natural organic matter and the expandability of clay
380   minerals on cesium adsorption and mobility. Geochim. Cosmochim. Acta 135,
381   49-65.

382 Franklin E.R. and Lee E. (1996) Synthesis and ion-exchange properties of Na-4-mica. J.
383   Mater. Chem. 6, 109-115.

384 Galambos M., Kufcakova J. and Rajec P. (2009) Adsorption of cesium on domestic
385   bentonites. J. Radioanal. Nucl. Chem. 281, 485-492.

386 Galunin E., Alba M.D., Santos M.J., Abrao T. and Vidal M. (2010) Lanthanide sorption
387   on smectitic clays in presence of cement leachates. Geochim. Cosmochim. Acta
388   74, 862-875.

389 García-Gutiérrez M.M., T.; Mingarro, M. (2010) Ensayos de sorción de 137Cs por la
390   muestra "rojo carbonero" para su empleo en la construcción de una barrera
391   reactiva permeable, CRI-9 (Huelva). CIEMAT, Madrid.

392 Garcia-Jimenez M.J., Cota A., Osuna F.J., Pavon E. and Alba M.D. (2016) Influence of
393   temperature and time on the Eu3+ reaction with synthetic Na-Mica-n (n=2 and
394   4). Chem. Eng. J. 284, 1174-1183.

395 Gregor M.C., B. (1969) Bentonite and its use. SAV, Bratislava.

396 Harter R.D. and Baker D.E. (1977) Applications and misapplications of Langmuir
397   equation to soil adsorption phenomena. Soil Sci. Soc. Am. J. 41, 1077-1080.

398 Kodama T., Harada Y., Ueda M., Shimizu K., Shuto K. and Komarneni S. (2001)
399   Selective exchange and fixation of strontium ions with ultrafine Na-4-mica.
400   Langmuir 17, 4881-4886.

401   Limousin G., Gaudet J.P., Charlet L., Szenknect S., Barthes V. and Krimissa M. (2007)

402   Sorption isotherms: A review on physical bases, modeling and measurement.

403   Appl. Geochem. 22, 249-275.

404   Linares J.H., F.; Cuadros, F.J. (1993) Comportamiento geoquímico de barreras

405   arcillosas: Transformaciones hidrotermales en esmectitas alúmicas. Estudios

406   Geol. 49, 127-136.

407   Nakao A., Thiry Y., Funakawa S. and Kosaki T. (2008) Characterization of the frayed

408   edge site of micaceous minerals in soil clays influenced by different pedogenetic

409   conditions in Japan and northern Thailand. Soil Sci. Plant Nutr. 54, 479-489.

410   Oztop B. and Shahwan T. (2006) Modification of a montmorillonite-illite clay using

411   alkaline hydrothermal treatment and its application for the removal of aqueous

412   Cs+ ions J. Colloid Interface Sci. 295, 303-309.

413   Park Y., Shin W.S. and Choi S.J. (2012) Removal of Co, Sr and Cs from aqueous

414   solution using self-assembled monolayers on mesoporous supports. Korean J.

415   Chem. Eng. 29, 1556-1566.

416   Paulus W.J., Komarneni S. and Roy R. (1992) Bulk synthesis and selective exchange of

417   strontium ions in Na4Mg6Al4Si4O20F4 mica. Nature 357, 571-573.

418   Pavon E., Castro M.A., Cota A., Osuna F.J., Pazos M.C. and Alba M.D. (2014)

419   Interaction of Hydrated Cations with Mica-n (n=2, 3 and 4) Surface. J. Phys.

420   Chem. C 118, 2115-2121.

421   Poinssot C., Baeyens B. and Bradbury M.H. (1999) Experimental and modelling studies

422   of caesium sorption on illite. Geochim. Cosmochim. Acta 63, 3217-3227.

423   Rani R.D. and Sasidhar P. (2012) Sorption of Cesium on Clay Colloids: Kinetic and

424   Thermodynamic Studies. Aquat. Geochem. 18, 281-296.

425   Sanz J. and Serratosa J.M. (1984) Si-29 and Al-27 high-resolution mas-nmr spectra of

426   phyllosilicates. J. Am. Chem. Soc. 106, 4790-4793.

427   Saxena A., Tomar R., Murali M.S. and Mathur J.N. (2003) Sorption of Am(III), U(VI)

428   and Cs(I) on sodium potassium fluorophlogopite, an analogue of the fluorine

429   mica mineral. J. Radioanal. Nucl. Chem. 258, 65-72.

430   Steinhauser G. (2014) Fukushima's Forgotten Radionuclides: A Review of the

431   Understudied Radioactive Emissions. Environ. Sci. Technol. 48, 4649-4663.

432   Takahashi M., Muroi M., Inoue A., Aoki M., Takizawa M., Ishigure K. and Fujita N.

433   (1987) Properties of bentonite clay as buffer material in high-level waste

434   geological disposal .1. Chemical-species contained in bentonite. Nucl. Technol.

435   76, 221-228.

436   Vejsada J., Hradil D., Randa Z., Jelinek E. and Stulik K. (2005) Adsorption of cesium

437   on Czech smectite-rich clays - A comparative study. Appl. Clay Sci. 30, 53-66.

438   Veli S. and Alyuz B. (2007) Adsorption of copper and zinc from aqueous solutions by

439   using natural clay. J. Hazard. Mater. 149, 226-233.

440   Villa-Alfageme M., Hurtado S., El Mrabet S., Pazos M.C., Castro M.A. and Alba M.D.

441   (2015) Uranium immobilization by FEBEX bentonite and steel barriers in

442   hydrothermal conditions. Chem. Eng. J. 269, 279-287.

443   Weir A.H. (1965) Potassium retention in montmorillonite. Clay Miner. 6, 17-22.

444   Wu J.J., Li B., Liao J.L., Feng Y., Zhang D., Zhao J., Wen W., Yang Y.Y. and Liu N.

445   (2009) Behavior and analysis of Cesium adsorption on montmorillonite mineral.

446   J. Environ. Radioact. 100, 914-920.

447   Xi J.H., He M.C. and Zhang G.Z. (2014) Antimony adsorption on kaolinite in the

448   presence of competitive anions. Environ. Earth Sci. 71, 2989-2997.

449   Zachara J.M., Smith S.C., Liu C.X., McKinley J.P., Serne R.J. and Gassman P.L. (2002)

450   Sorption of Cs+ to micaceous subsurface sediments from the Hanford site, USA.

451   Geochim. Cosmochim. Acta 66, 193-211.

452